Available online at www.sciencedirect.com

ScienceDirect

Acta Materialia 73 (2014) 177–185

Acta MATERIALIA

www.elsevier.com/locate/actamat

Experimental and numerical studies on friction welding of thixocast A356 aluminum alloy

Shailesh K. Singh [a], K. Chattopadhyay [a], G. Phanikumar [b], P. Dutta [c,*]

[a] Department of Materials Engineering, Indian Institute of Science, Bangalore 560012, India
[b] Department of Metallurgical and Materials Engineering, Indian Institute of Technology, Madras 600036, India
[c] Department of Mechanical Engineering, Indian Institute of Science, Bangalore 560012, India

Received 3 March 2014; received in revised form 9 April 2014; accepted 9 April 2014
Available online 7 May 2014

Abstract

This paper highlights the role of globular microstructure on the weldability of semi-solid processed aluminum alloys via high temperature flow behavior. The investigation was carried out on the joining of thixocast A356 aluminum alloy components by friction welding. A thermomechanical model was developed to predict the temperature and stress distributions, as well as to identify the suitable and safe range of parameters. Good comparisons between numerical and experimental results were observed. In addition, metallographic examinations and hardness and tensile tests of the welded samples were carried out. It was found that the tensile strength of the joint is higher than the tensile strength of the parent material for the optimum set of parameters.

Keywords: Friction welding; Temperature measurement; Constitutive equation; von Mises stress; Microstructure

1. Introduction

Aluminum–silicon alloys are widely used to cast high strength components in the aerospace and automobile industries with the primary aim of reducing weight and fuel consumption. However, porosity, brittle eutectic/secondary particles along dendrite boundaries and coarse primary dendrites in these alloys diminish the mechanical properties of the castings, particularly ductility, toughness and fatigue strength [1]. The aforementioned limitations reduce the potential of these cast alloys to be used as structural components under dynamic loading conditions [2]. Although forged products are superior in terms of mechanical properties, their applications suffer from the required increase of press capacity, short die life and forming limitations. To overcome the above problems, semi-solid manufacturing, which can produce parts close to near net shape along with superior mechanical properties, has been considered as a possible alternative. The joining of components processed through this route with conventional fusion welding creates voids, hot cracking, distortion in shape and more importantly the evolution of a dendritic microstructure that ultimately would lead to inferior mechanical properties of the weld region. Friction welding, which is essentially a solid state joining process, can be a promising alternative as it can avoid defects associated with melting and solidification present in a typical fusion welding process.

The process of friction welding can be classified as either continuous drive friction welding or inertia friction welding. In the present study, continuous drive friction welding was used. In this process, one of the parts is held stationary while the other is rotated at a constant speed. The fixed part is brought towards the rotary component and both parts are made to rub against each other. Due to the rubbing action, sufficient heat is generated, which softens the material at the interface. Subsequently, the motion of the

* Corresponding author.
E-mail address: pradip@mecheng.iisc.ernet.in (P. Dutta).

http://dx.doi.org/10.1016/j.actamat.2014.04.019
1359-6454/

rotary component is stopped and the axial pressure on the fixed part is increased to a higher forging pressure for the required upset time. The effect of forging pressure is to promote the mixing of the two materials, which consolidates the weld. The basic parameters of the friction welding process are therefore the friction pressure, friction time, rotational speed and forging pressure.

In studying friction welding, the problem that one usually faces is how to experimentally measure the temperature variation from the center to the periphery, as well as the stress developed during the process. Hence, modeling techniques are employed to understand the physical phenomena. Critical assessment of the literature on friction welding [3] indicates that only a limited number of studies are available that can model this process, taking temperature-dependent flow behavior and the evolving thermal profile due to plastic dissipation into account. Also, there are very few studies available on the weldability of semi-solid processed alloys [4–8]. The application of solid state welding on these kinds of materials, to the best of our knowledge, is completely unexplored. In the present study, friction welding of semi-solid processed A356 aluminum alloy has been modeled by taking into account the temperature-dependent flow properties. Hot compression tests were performed to determine the material parameters that describe the constitutional behavior of the semi-solid processed alloy. These data were subsequently used in the coupled thermal and stress models of the process. Simulation results were validated using experimental measurements of the thermal field near the weld interface during friction welding, using thermocouples as well as infrared imaging.

2. Experimental procedure

2.1. Procedure for thixocasting

The material investigated was A356 aluminum alloy, the chemical composition of which (in wt.%) is Si: 7.5; Mg: 0.4; Fe: 0.15; Cu: 0.03; Mn: 0.03; Ti: 0.2; Sr: 0.05; Ni: 0.03; and balance: Al. The material was received in the form of an ingot, with a dendritic microstructure as produced by a conventional casting technique. The thixocast samples with non-dendritic microstructure were produced in two steps: (a) production of non-dendritic microstructure billets with electromagnetic stirring and (b) processing of those billets to make components. In step (a), the ingots were melted and cooled to the pouring temperature, which was slightly above the liquidus temperature. The melt was then poured into an electromagnetic stirrer in which shearing action produced at the solid/liquid interface resulted in the formation of slurry, which, upon solidification, finally produced cylindrical billets with non-dendritic microstructure. In step (b), the cylindrical billets thus obtained were sectioned to the required size, reheated in the induction furnace to a semisolid (between solidus and liquid temperature) condition and immediately injected into a closed die, in a die casting machine, to obtain the required shaped component. Subsequently, samples extracted from runner bars of such components were used for hot compression testing and friction welding experiments.

2.2. Hot compression testing

In order to evaluate the constants of the constitutive equation, compression tests were carried out with strain rates ranging from 0.001 to 10 s^{-1}. Tests were carried out at strain rate values one order of magnitude apart and across a temperature range of 300–500 °C at 50 °C intervals, using a computer-controlled servohydraullic testing machine (DARTEC®) of 100 kN capacity. Specimens were prepared from a thixocast A356 alloy bar as well as a conventionally cast A356 ingot and machined in the form of a cylinder with a height-to-diameter ratio of 1.5 (height is 15 mm and diameter is 10 mm). The temperature of the specimen was monitored with a thermocouple embedded in a hole of 0.8 mm diameter drilled at half the height of the specimen. The specimen was deformed to 50%, corresponding to a true strain of 0.69. The load stroke curve obtained from the compression test was converted to the engineering stress–strain curve and subsequently to the true stress–strain curve using standard equations. The elastic region was subtracted from the true stress–strain curve to obtain the true stress–true plastic strain relation.

2.3. Friction welding experiment

The experiments were performed on the continuous drive friction welding machine. The experimental specimens were machined from thixocast A356 aluminum alloy component as well as conventionally cast A356 aluminum alloy components in the form of cylindrical bars of dimensions 85 mm length and 20 mm diameter.

2.4. Temperature measurement

Transient temperatures were measured at three locations within the stationary specimen during the welding process using K type thermocouples. Holes of 0.8 mm diameter were drilled at a spacing of 5 mm along the axial direction from the original contact section, as shown in Fig. 1. The thermocouples were beaded at the tip and stuck at the

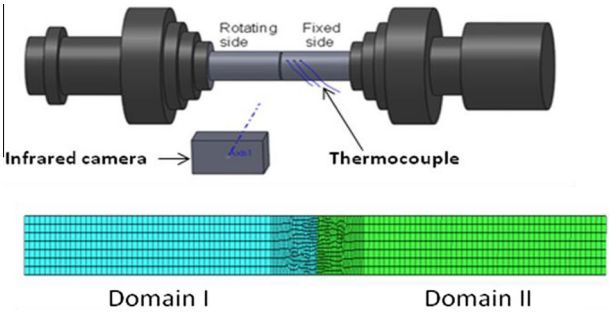

Fig. 1. Schematic view of geometrical model with thermocouple position and mesh geometry of the 2-D model.

measuring points with glue. A data acquisition system capable of acquiring 50,000 samples s^{-1} across 32 channels using a signal conditioner was used to connect the thermocouples with the computer where the temperature variations with time during friction welding were recorded.

In order to measure the temperature at the interface and its vicinity, infrared thermography, which is a non-contact temperature measuring method, was used. Thermography involves the detection of radiation in the electromagnetic spectrum with the wavelength ranging from 0.9 μm to 14 μm. In order to increase the accuracy of temperature measurement and to avoid reflection during temperature measurement, the samples were coated with black paint at the interface area and close to it.

2.5. Mechanical test and metallographic examinations

The mechanical properties of the welds were assessed using tensile and micro-hardness tests. In order to correlate the mechanical properties with the metallurgical characteristics, half- sections were taken for metallography of the weld interface. Besides optical microscopy, a scanning electron microscope (field emission tipped SERION, FEI make) was used for microstructural observation.

3. Numerical modeling

3.1. General assumptions

For the analysis of friction welding, isotropic material properties throughout the deformation process and temperature-dependent physical, thermal and mechanical properties were assumed. Due to axial symmetry, a two-dimensional (2-D) axisymmetric model was used in the present case.

3.2. Analysis

Temperature-dependent physical properties and mechanical properties as well as a viscoplastic constitutive equation were used in the model. The thermal and mechanical responses to the material during the friction welding process were investigated by finite element simulations. In this study, a coupled thermomechanical model was developed for analysis. First, a nonlinear, transient 2-D heat transfer model was developed to determine the temperature fields. Subsequently, the temperature fields were used as input to a nonlinear, 2-D structural model in order to predict the distortions and the von Mises stresses. The finite element model was parametrically built using APDL (ANSYS Parametric Design Language) provided by commercial software package ANSYS 12.1.

3.3. Heat generation

To predict the thermomechanical interaction during the friction welding process it is important to understand the phenomenon of heat generation during the process. Heat generation in friction welding depends on the contact condition between two workpieces. The contact condition during the friction welding process changes from sliding to sticking. According to the contact condition, heat generation rate is defined in three stages. In the initial stage when the temperature is low, friction shear stress is less than shear yield stress. Hence, at this stage, the sliding condition ($\delta = 0$) described by Coulomb friction was assumed, where δ is a state variable, which denotes the extent of sticking. At higher temperatures, shear yield stress becomes less than frictional stress (i.e. yield strength of the material decreases with rise in temperature) and contact is defined by the pure sticking condition. For the third situation, which is the transition from Coulomb friction to full plasticity at the interface, a partial sliding–sticking condition (i.e. $0 < \delta < 1$) was assumed. It was assumed that the transition from Coulomb friction ($\delta = 0$) to full plasticity ($\delta = 1$) takes place within a short duration [9,10].

When modeling the friction welding process, the contact condition is the most critical part of the numerical model. In the model, heat generation due to both sliding and sticking conditions was taken into account using a load step file. Heat generation due to transition from Coulomb friction ($\delta = 0$) to full plasticity ($\delta = 1$) (i.e. partial sliding and sticking) was ignored because of the assumption that this process takes place within a short duration [9], and its impact on heat generation will be negligible. In the sliding condition, the Coulomb law of friction is applied to describe the shear force between the workpieces. In general, the law estimates the contact shear stress as

$$\tau = \mu p \tag{1}$$

where μ is the friction coefficient and p is the contact pressure. Therefore the heat generated by friction between the workpiece is given by

$$q = \mu \cdot \omega \cdot p \cdot r \tag{2}$$

For hot working of aluminum alloys, the relationship between the shear stress and the yield flow stress at elevated temperatures can be expressed by the von Mises flow criterion [11]:

$$\mu = \frac{\tau}{\sigma} = \frac{1}{\sqrt{3}} \simeq 0.577 \tag{3}$$

From this it is seen that the use of a constant value for the friction coefficient (i.e. $\mu = 0.5$) is a reasonable assumption under the prevailing circumstances.

Therefore, while Coulombic friction controls the interface forces at low loads according to Amontons' law, the load and temperature increase to a point where the real area of contact is equal to the apparent area of contact (corresponding to sticking condition). The friction at this stage becomes independent of pressure and takes on the value τ_y, which is the shear yield stress of the workpiece material. For such a situation, heat generation is given by

$$q = \tau_y \omega r \tag{4}$$

3.4. Thermal model

The purpose of the thermal model is to calculate the transient temperature fields developed in the workpieces during friction welding. Due to axial symmetry, a 2-D heat-transfer model was adequate for the present case. Both domains were meshed using Plane 55, which is a 2-D solid element with four nodes having the temperature as a single degree of freedom at each node (Fig. 1). A very fine mesh was created near the weld zone, with element size increasing with distance from the weld. The weld interface is subjected to high temperature gradient and distortion, and hence the fine mesh will be able to capture the physics better. An advantage of using the Plane 55 element is that the element can be replaced by an equivalent structural element for structural analysis. Moreover, the additional advantage of this element is that it supports adaptive meshing. The adaptive meshing manages the mesh distortion if the deformation becomes large during the process.

To facilitate the numerical solution of the thermal problem, heat-transfer coefficients need to be determined. Since domain I is rotating at high speed, it experiences forced convection cooling for, which the correlation for Nusselt number is [12]:

$$Nu = \frac{hD}{k} = C\,\mathrm{Re}_D^m\,\mathrm{Pr}^{1/3} \tag{5}$$

An estimate for the heat transfer coefficient for the rotating part comes out as:

$$h_r = 23.5\ \mathrm{W\,m^{-2}\,^\circ C^{-1}}$$

Domain II, being stationary, experiences cooling by free convection, for which the heat transfer coefficient is significantly lower. The corresponding correlation for the Nusselt number is given by [13]

$$Nu = \frac{h_f D}{k} = \left[0.6 + \frac{0.387 Ra_D^{1/6}}{\left[1 + (0.599/\mathrm{Pr})^{9/16}\right]^{8/27}}\right]^2 \tag{6}$$

An estimate for the heat transfer coefficient for the stationary part, using above correlation, comes out as:

$$h_f = 14.5\,\frac{\mathrm{W}}{\mathrm{m^2\,^\circ C}}$$

The above two relations of heat transfer coefficient are further used for the numerical solution of temperature profiles in domains I and II.

3.5. Mechanical model

The second step in the thermomechanical analysis is the development of the mechanical model. The temperature distributions obtained from the thermal analysis are used as the input to the mechanical model. This model is used to estimate the stress distribution during the welding process. A structural element defined by eight nodes (i.e., Plane 182) having three degrees of freedom at each node is used. This element is capable of supporting plasticity, stiffness, large deflection and strain. In the present analysis, the heat transfer model containing the equivalent thermal element Plane 55 is replaced by Plane 182 by switching the element type from thermal to structural. The benefit of using this element type is that the temperature field obtained from thermal step can be applied as loads at the nodes. This element exhibits similar geometry, node locations and coordinate as the Plane 55 element. An identical mesh pattern generated for the thermal analysis is used in the structural analysis.

3.6. Flow stress and constitutive model

Analysis of the flow behavior of material is necessary before selecting the constitutive equation for flow stress prediction. Therefore, a study of the nature of the flow curves of the materials under investigation is required in the specified domain before selecting a suitable material model. The flow curves obtained for thixocast A356 and conventionally cast alloy of the same for two extreme temperatures (300 and 500 °C) at strain rate of 1 s^{-1} are presented in Fig. 2.

From the analysis of flow behavior of the materials under consideration, it is clear that both materials being studied show the phenomena of strain hardening, thermal softening, strain rate hardening and an effect of temperature and strain rate on flow stress. Elastic effects are negligible compared with local plastic deformation. In these conditions, a Johnson–Cook constitutive law is adapted to simulate the hot working of the metal [14]. It may be written in the following form:

$$\sigma = [A + B(\varepsilon)^n][1 + C\ln(\dot{\varepsilon}^*)][1 - (T^*)^m] \tag{7}$$

where σ is the von Mises flow stress; A represents the proof stress at reference temperature and strain rate; B is the coefficient of strain hardening; n is the strain hardening exponent; ε is the equivalent plastic strain; $\dot{\varepsilon}^* = \dot{\varepsilon}/\dot{\varepsilon}_0$ is the dimensionless strain rate, where $\dot{\varepsilon}$ is the strain rate and $\dot{\varepsilon}_0$

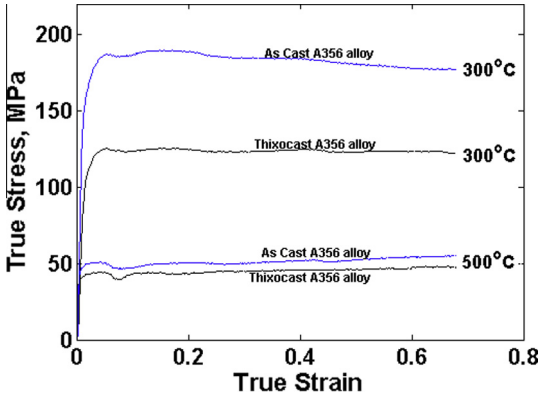

Fig. 2. True stress–true strain curves of thixocast and conventionally cast A356 aluminum alloy during hot compression deformation at $\dot{\varepsilon} = 1\ s^{-1}$.

Table 1
Parameters of the Johnson–Cook Model for thixocast and conventionally cast A356 aluminum alloy.

Parameters	Thixocast A356 alloy	Conventional cast A356 alloy
A	114.64 ± 1 (MPa)	153.94 ± 1 (MPa)
B	36.56 ± 0.6 (MPa)	25.06 ± 0.8 (MPa)
n	0.0243 ± 0.01	0.1351 ± 0.03
m	0.7469 ± 0.1	0.6717 ± 0.1
C	0.0707 ± 0.02	0.0799 ± 0.02

is the reference strain rate; T^* is the homologous temperature and is expressed as:

$$T^* = \frac{T - T_{ref}}{T_m - T_{ref}} \tag{8}$$

where T is the current absolute temperature, T_m is the melting temperature and T_{ref} is the reference temperature ($T \geqslant T_{ref}$). Room temperature or the minimum temperature of the text matrix can be taken as the reference temperature. C and m are the material constants termed strain rate sensitivity coefficient and thermal softening coefficient, respectively. The material constants involved in the equation are calculated from curve fitting of experimental data obtained through isothermal hot compression tests performed in the temperature range of 300–500 °C and strain rate in the range of 0.001–10 s^{-1}. The parameters obtained for thixocast A356 alloy and conventionally cast A356 aluminum alloy are shown in Table 1.

4. Results and discussion

4.1. Temperature and stress distribution

Temperature variations during the friction welding process were studied both numerically and experimentally. Fig. 3 represents the numerically estimated temperature distribution across the interface at various locations (i.e. center, mid-radius and surface). The numerical results reveal that the temperature at the center is less than at the mid-radius and the surface because heat generation is linearly proportional to the distance from the centerline. However, the convection cooling effect limits the temperature at the surface and its vicinity. The temperature distribution across the interface is not exactly symmetrical, due to different values of heat transfer coefficient used for the rotating and fixed sides. Similarly, radial distribution of temperature for various durations, as shown in Fig. 4, is obtained numerically. It indicates the duration of friction welding operation required to achieve a temperature needed for the welding process for a particular set of parameters. The above results showing temperature rise with time were obtained for parameters $\omega = 1000$ rpm, friction pressure = 60 MPa, upset time = 5 s and forging pressure = 110 MPa. A similar behavior is noticed for other sets of parameters as well.

In order to measure temperature along the axial direction, K-type thermocouples were used. The measured

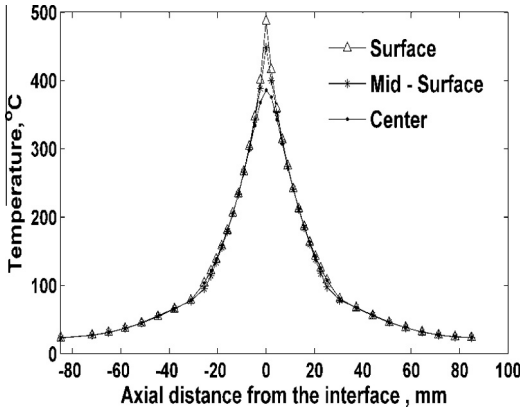

Fig. 3. Temperature distribution across the interface during friction welding of thixocast A356 aluminum alloy at various locations (i.e. center, mid-radius and surface).

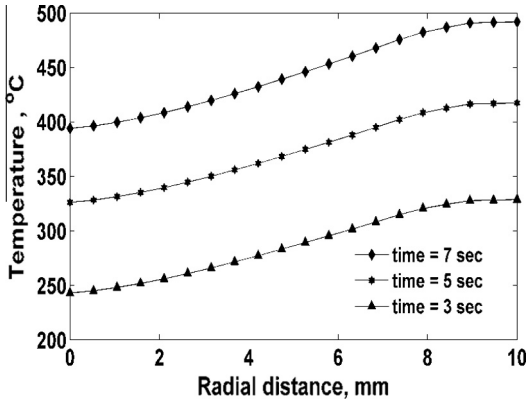

Fig. 4. Radial distribution of temperature for different durations during friction welding of thixocast A356 aluminum alloy.

temperatures at these locations are to be compared with the predictions from numerical simulation. Fig. 5 shows the predicted and measured temperatures along the axial direction for $z = 5$, 10 and 15 mm from the original weld interface during friction welding of thixocast A356 alloy. Some differences are observed between the numerical prediction and experimental measurement. This is due to the fact that during the burn-off stage, hot material at the weld interface is forced radially outward to form the flash, while fresh material is constantly brought to the weld interface by the relative axial displacement of the two workpieces. As a consequence, all embedded thermocouples were displaced towards the weld interface. This slight shift in thermocouple positions leads to differences in measured and predicted temperatures. Hence, in order to measure the temperature at the interface, infrared thermography, which is a non-contact temperature measuring method, was used.

Fig. 6a and b shows the contour plot of surface temperature distribution at the interface, as recorded by an infrared camera during friction welding of thixocast A356 aluminum alloy and conventionally cast A356 aluminum alloy, respectively. Both samples show similar temperature plots and comparable maximum temperature achieved

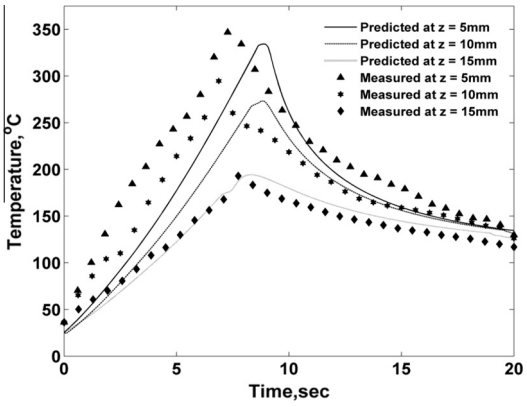

Fig. 5. Predicted and measured temperatures along the axial direction at a distance of 5, 10 and 15 mm from the original weld interface during friction welding of thixocast A356 alloy.

during welding with the same set of parameters. A similar comparison between numerical and experimental results is shown in Fig. 7a for temperature variation with time at the interface, and Fig. 7b shows the temperature profile along the axial direction. The comparisons between experiment and numerical results are found to be good.

Numerical simulation can be a suitable tool for estimating the stress distribution during the welding process, which is difficult to determine experimentally. The objective is mainly to help arrive at the parameters which would minimize the induced stress. Fig. 8a shows the von Mises stress profile of thixocast A356 alloy. At locations far away from the weld interface, the stress value is found to be close to that of the material at room temperature and the effects of temperature and deformation on material are negligible. Very close to the weld interface that is subjected to a large temperature rise during the welding process, the yield stress decreases. This, in turn, reduces the von Mises stress. However, at a little distance away from the weld interface, the plastic deformation is resisted by the surrounding colder material, and this in turn increases the von Mises stress. Similar behavior is also observed for conventionally cast A356 alloy. However, the magnitude of equivalent stress induced during friction welding process of conventional cast A356 alloy is higher compared to that of thixocast A356 alloy for the same set of parameters. This difference can be attributed to their different constitutive behavior at elevated temperature (Fig. 2). The flow curve analysis shows that flow stress of thixocast alloy is lower than that of the conventionally cast alloy at an elevated temperature for the same rate of deformation, indicating a better plastic flow property of thixocast alloy. Similarly Fig. 8b shows the von Mises stress distribution along the radial direction at the interface for thixocast A356 alloy and conventionally cast A356 alloy. It indicates that the there is a gradual drop in the magnitude of von Mises stress towards the periphery for both friction welded thixocast and conventionally cast A356 alloy. This is due to the fact the heat generation is proportional to the distance from the centerline; hence

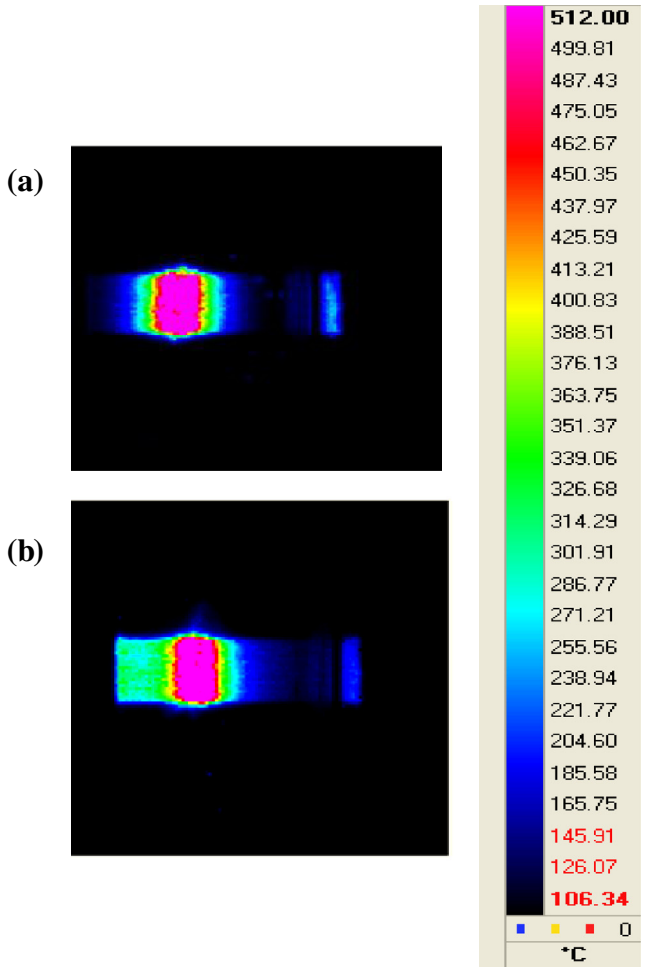

Fig. 6. Surface temperature distribution along the interface obtained by infrared thermography during friction welding of (a) thixocast A356 alloy and (b) conventionally cast A356 alloy.

the periphery would have a higher temperature than at the center. Consequently, the von Mises stress induced during welding at the periphery would be lower than that of the center; flow stress decreases with rise in temperature. Thus, this study highlights the role of the initial microstructure on the weldability of semi-solid processed alloys via the high temperature flow behavior. The results indicate a better response of the thixocast component towards friction welding.

4.2. Microstructure study

The heat generated in friction welding at the interface due to thermomechanical processing when dissipated through the parent material would result in a temperature gradient causing zones of material with a different microstructure. Microstructure evolution in the heat affected zone (HAZ) is evident from the distinct regions classified here as fully plasticized zone, partially deformed zone and undeformed zone. The friction welded joints were sectioned along the axis and observed using an optical

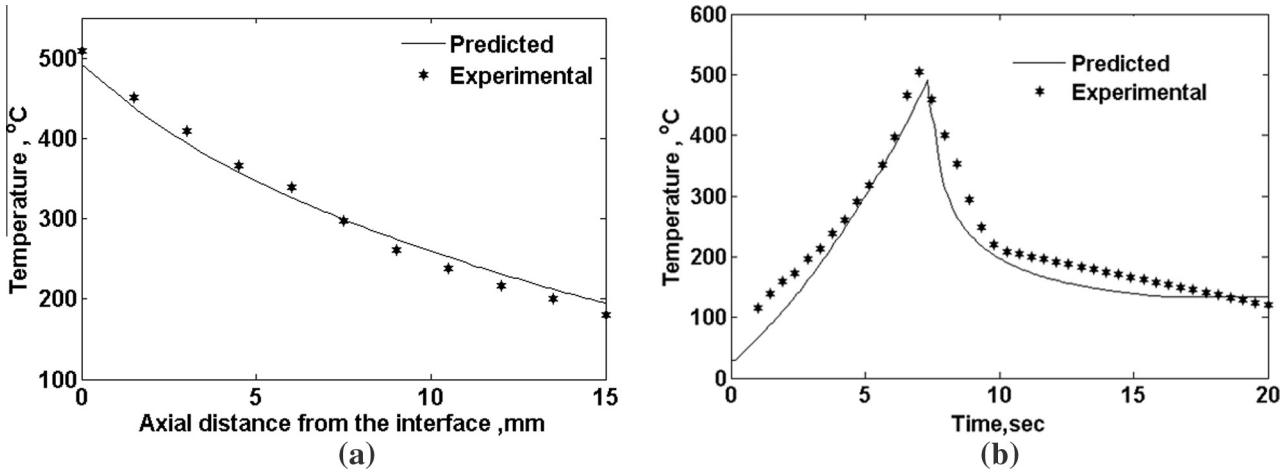

Fig. 7. Comparisons between numerical and experimental results for (a) temperature variation with time at the interface and (b) temperature variation along axial direction.

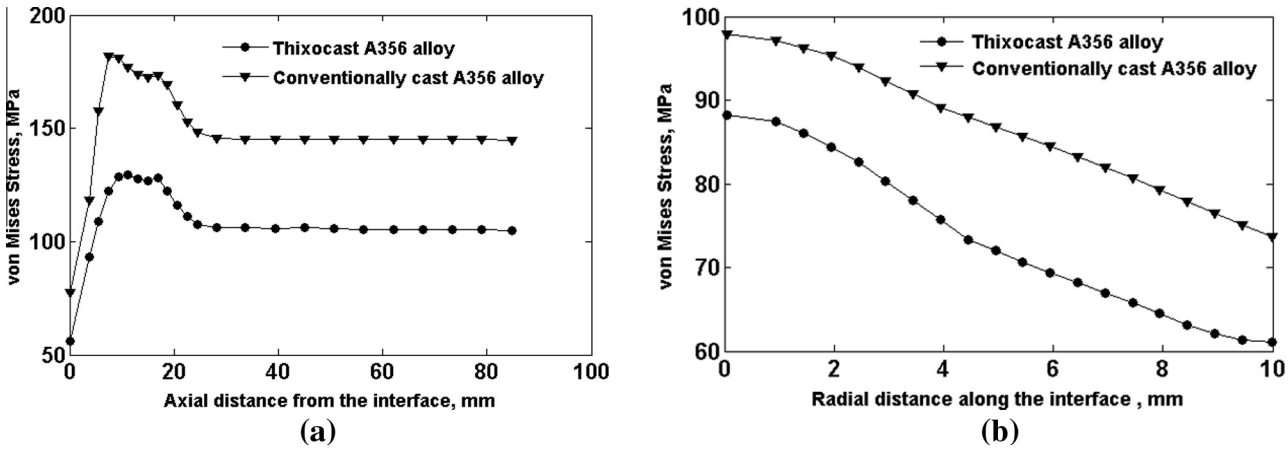

Fig. 8. Variation of von Mises stress distribution during friction welding: (a) in axial direction from the interface and (b) in radial direction along the interface for thixocast and conventionally cast A356 aluminum alloy, respectively.

microscope and a scanning electron microscope. Typical optical micrographs observed at the weld metal, HAZ and base metal of the thixocast A356 welded specimen are presented in Fig. 9a. The grain structure at the interface is finer compared to that of the base metal. The grain size of the α-phase at the interface is of the order of 0.7 μm, which is approximately two orders of magnitude smaller than that of the base metal having a grain size of 68 μm. These fine and equiaxed grain structures evolved by the recrystallization process during welding, as the welded materials near the interface were simultaneously subjected to frictional heat and plastic deformation. Therefore, the original grains were severely broken and dynamic recrystallized grains were generated during the welding process. The region adjacent to the fully plasticized zone shows an elongated grain structure normal to the direction of the compressive force. This structure seems to be dynamically recovered and repolygonization of the microstructure was observed. The region close to the partially deformed zone is the undeformed zone, which was not subjected to substantial thermo-mechanical effect. This zone is characterized by parent material microstructure having a globular α-phase. The impact of friction welding on eutectic phase of thixocast A356 alloy can be seen in the SEM image taken at higher magnification, as shown in Fig. 9b. At the interface, eutectic silicon forms fine globular particles, while in the partially deformed zone the silicon morphology consists of polyhedral silicon and fine lamellar and fibrous morphology. In the undeformed zone silicon appears in the form of coarse, sharp fibers. It is interesting to note that friction welding has led to a modification of silicon morphology that is otherwise possible only by suitable alloying elements during casting.

4.3. Hardness variations

The joint strength can be related to the hardness variation within the HAZ. Hardness variation was obtained using a 100 g load by the Vickers micro-hardness testing method. The hardness distribution assists in the

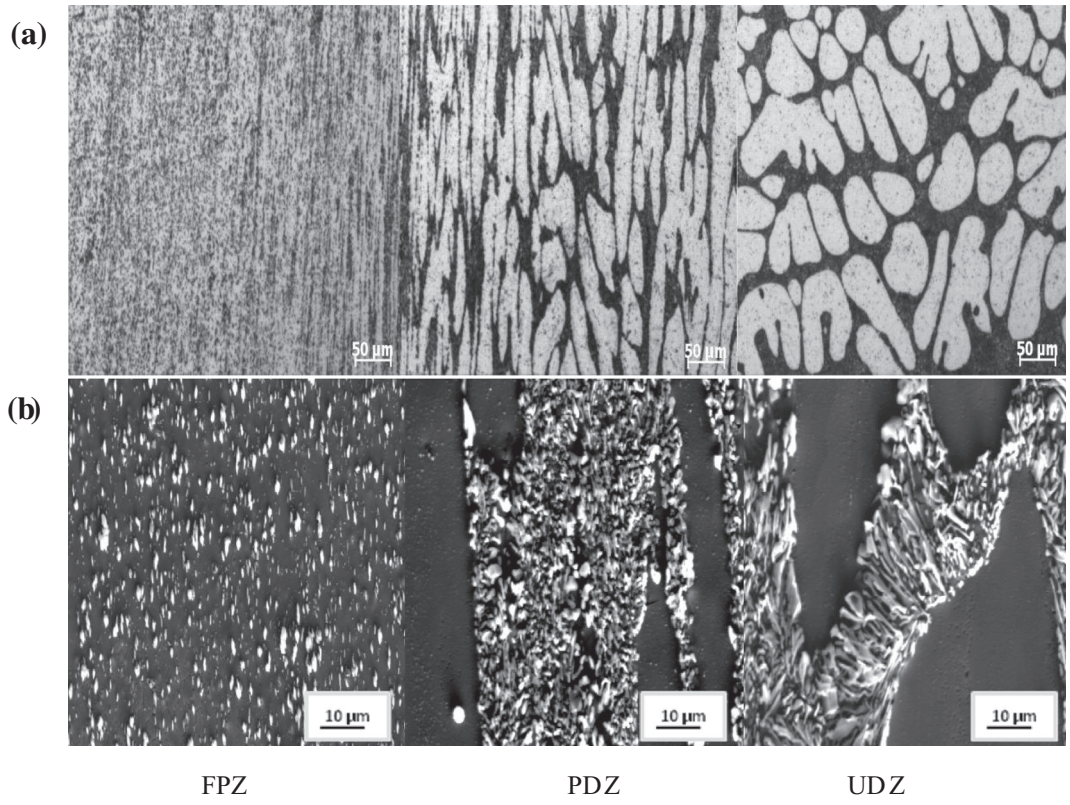

Fig. 9. Typical (a) optical micrographs and (b) SEM image observed at fully plasticized zone (FPZ), partially deformed zone (PDZ) and undeformed zone (UDZ) of thixocast A356 welded specimen.

interpretation of the weld microstructures and mechanical properties of the materials. As it can be seen from Fig. 10, maximum hardness values of joints appear at the weld interface and in its close vicinity (up to 0.3 mm on either side of the interface). This zone is characterized by severe plastic deformation where the grains are very fine due to effect of dynamic recrystallization. However, a little further away in the partially deformed zone, grains become elongated in the direction of the material flow, and the material undergoes repolygonization, which keeps the grain dimensionally stable and equiaxed. As such, there is a reduction in dislocation that decreases hardness in this region. Close to the partially deformed zone is the undeformed zone where hardness is found to be similar to that observed for the parent material. The effect of temperature and deformation is not significant in this region.

A similar observation is also recorded for the case of a conventionally cast A356 welded specimen, as shown in Fig. 10. On comparing the hardness of the two welded specimens, it is clear that the thixocast counterpart exhibits higher hardness, thus indicating a better weld metal property of thixocast alloy.

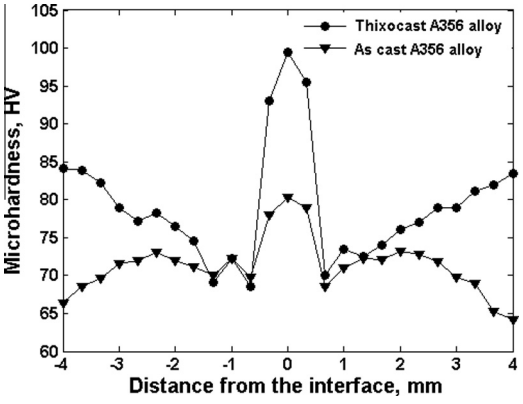

Fig. 10. Hardness variation along horizontal direction through interface for thixocast friction welded specimen and conventional cast friction welded specimen.

4.4. Tensile test

Tests for tensile strength of the joints were carried out in a Zwick® Universal Testing Machine of 100 t capacity. Comparisons of tensile properties between friction welded thixocast A356 alloy, unwelded thixocast A356 alloy, friction welded conventional cast A356 alloy and unwelded conventionally cast A356 alloy are shown in Fig. 11. Friction welded thixocast A356 alloy shows maximum tensile strength (229 MPa) followed by unwelded thixocast base A356 alloy (212 MPa), which is followed by friction welded conventionally cast A356 alloy (184 MPa). The base conventional cast alloy (176 MPa) depicts the minimum tensile strength. This is due to the fact that in the case of friction

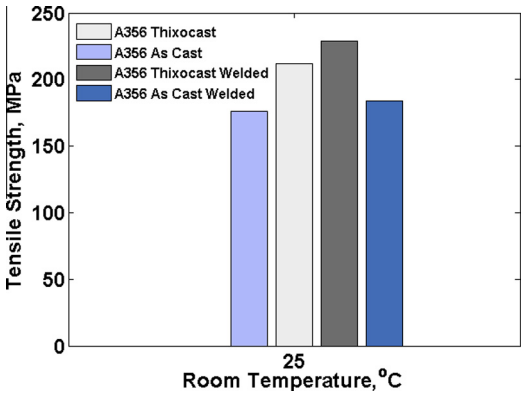

Fig. 11. Bar chart showing tensile strength of friction welded thixocast and conventional cast A356 alloy as well as not welded thixocast and conventional cast A356 alloy.

welding, fine grains are observed due to plastic deformation at the interface. This enhances the mechanical properties of the welded joint as compared to the parent material.

5. Conclusion

In this work, the application of friction welding on thixocast A356 alloy has been studied. Among the major findings, it is observed that flow data of A356 alloy could be used to model the friction welding process realistically, and thermal profiles predicted from simulation compare well with the experimentally measured ones. The magnitude of von Mises stress distribution during welding for the thixocast A356 sample is found to be lower than that of the conventionally cast sample, which is attributed to the difference in constitutive behavior at elevated temperature. Also, hardness profile and tensile studies indicate that the HAZ of friction welded samples of thixocast alloys is stronger than the corresponding base material. Overall, the study proves the viability of friction welding as a possible means of joining aluminum alloys cast in the form of a non-dendritic microstructure.

Acknowledgements

We acknowledge the support of CNDE (Centre for Non Destructive Evaluation) at IIT Madras. We cordially thank Prof. K. Balasubramaniam and Libin for their help in measuring temperature with an infrared camera during the friction welding experiment.

References

[1] Ma ZY, Pilchak AL, Juhas MC, Williams JC. Scr Mater 2008;58:361.
[2] Cavaliere P, De Marco PP. Mater Sci Eng A 2007;462:393.
[3] Maalekian M. Sci Technol Weld Joining 2007;12:738.
[4] D'Alvise L, Massoni E, Wallae SJ. J Mater Process Technol 2002;125:387.
[5] Sandhya S, Phanikumar G. Mater Sci Forum 2013;765:751.
[6] Toit DM, Letsoalo P, Moller H. Solid State Phenom 2012;192:161.
[7] Singh SK, Chattopadhyay K, Dutta P. Solid State Phenom 2013;192:305.
[8] Boonchouytan W, Ratanawilai T, Muangjunburee P. Adv Mater Res 2012;488:328.
[9] Maalekian M, Kozeschnik E, Brantner HP, Cerjak H. Acta Mater 2008;56:2843.
[10] Khalid Rafi H, Balasubramaniam K, Phanikumar G, Prasad Rao K. Metall Trans A 2011;42:3425.
[11] Dieter GE. Mechanical metallurgy. New York: McGraw-Hill; 1986.
[12] Hilpert R. Forsch Geb Ingenieurwes 1933;4:215.
[13] Churchill SW, Chu HHS. Int J Heat Mass Transfer 1975;18:1323.
[14] Johnson GJ, Cook WH. Proceedings of the seventh international symposium on ballistics. The Hague; 1983. p. 541.